JOURNAL OF GEOPHYSICAL RESEARCH, VOL. 104, NO. D16, PAGES 19,039–19,055, AUGUST 27, 1999

Climate model simulation of winter warming and summer cooling following the 1991 Mount Pinatubo volcanic eruption

Ingo Kirchner,[1] Georgiy L. Stenchikov,[2] Hans-F. Graf,[1]
Alan Robock,[2] and Juan Carlos Antuña[2]

Abstract. We simulate climate change for the 2-year period following the eruption of Mount Pinatubo in the Philippines on June 15, 1991, with the ECHAM4 general circulation model (GCM). The model was forced by realistic aerosol spatial-time distributions and spectral radiative characteristics calculated using Stratospheric Aerosol and Gas Experiment II extinctions and Upper Atmosphere Research Satellite-retrieved effective radii. We calculate statistical ensembles of GCM simulations with and without volcanic aerosols for 2 years after the eruption for three different sea surface temperatures (SSTs): climatological SST, El Niño-type SST of 1991-1993, and La Niña-type SST of 1984-1986. We performed detailed comparisons of calculated fields with observations. We analyzed the atmospheric response to Pinatubo radiative forcing and the ability of the GCM to reproduce it with different SSTs. The temperature of the tropical lower stratosphere increased by 4 K because of aerosol absorption of terrestrial longwave and solar near-infrared radiation. The heating is larger than observed, but that is because in this simulation we did not account for quasi-biennial oscillation (QBO) cooling and the cooling effects of volcanically induced ozone depletion. We estimated that both QBO and ozone depletion decrease the stratospheric temperature by about 2 K. The remaining 2 K stratospheric warming is in good agreement with observations. By comparing the runs with the Pinatubo aerosol forcing with those with no aerosols, we find that the model calculates a general cooling of the global troposphere, but with a clear winter warming pattern of surface air temperature over Northern Hemisphere continents. This pattern is consistent with the observed temperature patterns. The stratospheric heating and tropospheric summer cooling are directly caused by aerosol radiative effects, but the winter warming is indirect, produced by dynamical responses to the enhanced stratospheric latitudinal temperature gradient. The aerosol radiative forcing, stratospheric thermal response, and summer tropospheric cooling do not depend significantly on SST. The stratosphere-troposphere dynamic interactions and tropospheric climate response in winter are sensitive to SST.

1. Introduction

The effect of volcanic eruptions on atmospheric turbidity and the Earth's radiative balance contributes significantly to natural climate variability. Volcanic signals are episodic but can be very strong. The impact of strong volcanic eruptions on atmospheric radiative and chemical properties can cause intensive nonlinear responses in the climate system. Climate feedback mechanisms produce a wide spectrum of inherent variability in the response. Therefore it is difficult to isolate the contributions of different factors on climate variability on the seasonal time scale.

Volcanic activity includes continuous moderate emissions into the troposphere [*Graf et al.*, 1997] and intensive eruptions that inject material into the lower stratosphere. The lifetime of volcanic aerosols depends on the atmospheric meteorological conditions and the placement of the erupted material. In the troposphere, volcanic aerosols are concentrated near the emission regions because of effective removal processes. In the stratosphere a globally distributed layer of sulfate aerosols, the Junge layer [*Junge et al.*, 1961], is observed. Strong perturbations of this layer are produced by violent volcanic eruptions, while its background state is maintained by a permanent supply of tropospheric sulfur species (COS, SO_2) from different sources.

Violent eruptions inject tens of megatons of sulfuric gases and ash particles into the atmosphere above the tropopause during a few days or hours. The relatively large ash particles are removed from the stratosphere by dry sedimentation during a couple months, and can cause significant climate perturbation only under specific conditions [*Robock et al.*, 1995]. Sulfuric gas converts into optically active long-lived sulfate aerosol, which perturbs the radiative and chemical balances of the climate system. The aerosol cloud decays exponentially with a characteristic time of about 1 year, influencing climate during 3-4 years following the eruption.

[1]Max Plank Institute for Meteorology, Hamburg, Germany.
[2]Department of Environmental Sciences, Rutgers University, New Brunswick, New Jersey.

Paper number 1999JD900213.
0148-0227/99/1999JD900213$09.00

The two strongest eruptions of the century were El Chichón in April 1982 and Mount Pinatubo in June 1991, with Pinatubo the strongest and best documented event of the century so far. For several years following these events, statistically significant changes of the global temperature and circulation were observed [*Robock and Mao*, 1995; *Mao and Robock*, 1998]. Global sulfur emission of volcanoes to the troposphere is about 14% of the total natural and anthropogenic emission [*Graf et al.*, 1997], produced mostly by silent and weak explosive volcanoes. Radiative forcing from such emissions is about -0.21 W/m^2 for the globe and -0.31 W/m^2 for the Northern Hemisphere (NH). In addition to this continuous forcing, violent eruptions cause sporadic disturbances of the Earth's radiative balance more than 1 order of magnitude larger [*Minnis et al.*, 1993]. *Robock and Free* [1995] describe the record of volcanism of the past 150 years.

Volcanic sulfate aerosols are purely scattering in the ultraviolet (UV) and visible solar bands. Absorption becomes significant only in the middle of the near-infrared (near-IR) interval between 2 and 3 μm. Scattering aerosols in the stratosphere reduce the amount of total shortwave (SW) solar radiation absorbed by the Earth and slightly increase gascous absorption in the atmosphere because of a longer photon path [*Lacis and Mishchenko,* 1995]. Aerosol absorption of solar near-IR and outgoing longwave (LW) radiation heats the stratosphere, but reduction of downward radiation at the tropopause cools the troposphere and underlying surface. The total (SW+LW) top of the atmosphere radiative forcing due to submicron sulfate aerosols is negative [*Stenchikov et al.*, 1998].

Volcanic aerosol heating in the tropical lower stratosphere produces a perturbation of the temperature gradient, resulting in an enhanced North Polar vortex in the lower stratosphere and strengthening of the westerlies in the winter [*Kodera et al.*, 1991; *Kodera*, 1994; *Graf et al.*, 1994]. A coupling between the stratosphere and troposphere, forced by interaction of the mean flow with large-scale planetary waves, causes the dynamic signal to penetrate downward and modifies the tropospheric circulation patterns [*Charney and Drazin,* 1961; *Boville*, 1983]. This dynamic feedback mechanism produces winter warming and provides a very important contribution to the resulting climate change [*Robock and Mao*, 1992, 1995; *Graf et al.*, 1993; *Kirchner and Graf*, 1995; *Mao and Robock*, 1998].

Observations show that the enhanced stability of the North Polar vortex is correlated with strengthening of the North Atlantic Oscillation (NAO) pattern. NAO is one of the fundamental natural circulation modes. *Perlwitz and Graf* [1995] called this type of circulation the baroclinic mode. This circulation pattern is preferred during winters following violent volcanic eruptions [*Graf et al.*, 1994] and produces, during its strong vortex phase, a winter warming pattern over Eurasia. The evolution and generating mechanisms of this mode are not well understood.

Volcanic aerosols produce chemical forcing in the stratosphere because they change stratospheric temperatures and photolysis rates and provide a surface for heterogeneous reactions. Therefore the stratospheric chemical structure is disturbed [*Crutzen*, 1976; *Tabazadeh and Turco*, 1993; *Tie and Brasseur*, 1995; *Tie et al.*, 1996; *Solomon et al.*, 1996]. The most important chemical effect is on ozone destruction in middle and low latitudes, caused by heterogeneous reactions with anthropogenic chlorine species. Activation of ClO_x on aerosol surfaces effectively reduces the concentration of ozone at all times of the year in proportion to the available aerosol surface area. The ozone reduction caused by this process reaches about 5% in midlatitudes [*Zerefos et al.*, 1994; *Tie et al.*, 1996; *Coffey*, 1996]. The chemical ozone destruction is less effective in the tropics, but lifting of low ozone concentration layers with the aerosol cloud [*Kinne et al.*, 1992] causes a fast decrease in ozone mixing ratio in the low latitudes. Observations show that the column ozone concentration changes from 2% in the tropics to 7% in the midlatitudes [*Angell*, 1997a]. The column ozone depletion is concentrated in a thin layer where the aerosols are injected. Therefore ozone depletion in the aerosol cloud is much larger and reaches 20% [*Grant et al.*, 1992; *Grant*, 1996]. Decrease of the ozone concentration causes less UV absorption in stratosphere, which modifies the aerosol heating effect [*Kinne et al.*, 1992, *Rosenfield et al.*, 1997].

In our earlier perpetual January experiment with coarse definition of the forcing and with the low resolution (T21) ECHAM2 general circulation model (GCM) [*Kirchner and Graf*, 1995], the circulation response in January following volcanic eruptions was fairly well simulated. The intensified polar vortex in the lower stratosphere led to an enhanced tropospheric westerly wind over the North Atlantic, and the temperature in the lower troposphere corresponded to the winter-warming pattern [*Robock and Mao*, 1992, 1995], but the temperature anomalies were too far poleward [*Graf et al.*, 1993]. Here we address the same problem in more detail with an improved model, in an experiment with better defined aerosol parameters [*Stenchikov et al.*, 1998], interactive calculation of the aerosol radiative effects, and an improved GCM (ECHAM4), including the full seasonal cycle.

The goal of this study is to improve the simulation of the observed dynamic response with a more realistic model and to reveal the sensitivity of the atmospheric response to the variations of the background circulation caused by different SSTs. Therefore we conducted three series of experiments for the 2 years after the eruption with climatological, El Niño-type, and La Niña-type sea surface temperatures (SSTs), and performed a detailed comparison with observations. For all cases, we performed ensembles of experiments with different restart conditions. We also estimate the contributions of other important factors like ozone depletion and the quasi-biennial (QBO) cycle.

2. Climate Model

The experiments were performed with the latest version of the Hamburg climate model ECHAM4. ECHAM4 is based on the weather forecast model of the European Centre for Medium-Range Weather Forecasting (ECMWF) and was adapted for climate simulations in Hamburg at the Max Planck Institute for Meteorology. Most of the changes between the ECMWF model and ECHAM are described by *Deutsches Klimarechenzentrum* [1994] for the previous model version, ECHAM3. *Roeckner et al.* [1996a] describe changes in the numerics and the physics between versions 3 and 4. ECHAM4 incorporates the modified Morcrette radiative scheme with explicit treatment of the radiative effects of aerosols [*Morcrette,* 1984; *Morcrette and Fouquart,* 1985; *Morcrette et al.*, 1986]. Radiative transfer is divided into six spectral regions in the longwave, and the

Table 1. Spectral Resolution of the ECHAM4 Radiation Scheme.

Band	Wavelength, μm	Description
1	5.3-6.9, 28.6-∞	LW, water vapor absorption
2	12.5-20.0	LW, CO_2 absorption
3	8.0-9.0, 10.3-12.5	LW, window
4	9.0-10.3	LW, ozone absorption
5	20.0-28.6	LW, window
6	3.6-5.3, 6.9-8.0	LW, water vapor absorption
7	0.2-0.68	SW, Solar UV and Visible
8	0.68-4.0	SW, Solar near IR

LW, longwave; SW, shortwave; UV, ultraviolet; IR, infrared.

solar part is divided into the visible and near-infrared bands (Table 1). Absorption due to CH_4, N_2O, CFCs, and O_3 is included with a modified treatment of the H_2O continuum absorption [*Giorgetta and Wild*, 1995]. The radiative effects of cloud droplets (water and ice) and aerosol particles are accounted for.

We use the T42L19 version of ECHAM4. The spatial resolution is based on a 42 spherical harmonic expansion with triangular truncation (roughly equivalent to a latitude-longitude grid of 2.8°×2.8°) and 19 vertical layers with sigma-pressure hybrid vertical coordinates. We used standard reference runs with climatological SST and observed SST from Atmospheric Model Intercomparison Project [*Gates*, 1992] calculations for the period from 1979 to 1993 [*Stendel and Bengtsson*, 1997]. Initial conditions for our experiments were taken from these standard runs. For the period 1979-1988 the AMIP SST data set was used, and from 1989 to 1993 the SSTs were obtained from the U.S. National Meteorological Center [*Reynolds*, 1988]. On the basis of this SST data set, the climatological annual cycle of SST was calculated and used as the boundary condition for a 15-year control experiment. The second reference experiment was performed using the 15-year actual observed SST.

Aerosol parameters were calculated using a Mie code [*Wiscombe*, 1980]. *Stenchikov et al.* [1998] discuss the direct radiative forcing of the Pinatubo aerosols. Because of reflection of solar radiation by the aerosol cloud, the net solar flux decreases at the surface by 5-6 W/m^2 under the thickest part of the cloud in the tropics, in good agreement with satellite and ground-based observations. Absorption of near-IR and LW radiation by the aerosols produces heating of up to 0.3 K/d in the tropical lower stratosphere. In the troposphere, the aerosols produce a cooling of only about −0.01 K/d. Aerosol radiative forcing is not sensitive to variations of atmospheric parameters and SSTs [*Stenchikov et al.*, 1998].

The aerosol data set contains aerosol extinction, single scattering-albedo, and asymmetry factor for the first day of each of the 24 months following the Pinatubo eruption, starting from June 1, 1991, on the ECHAM4 spatial grid. We interpolated the aerosol parameters in time for each radiative time step. The aerosol parameters are in zonal-mean form, but the optical depth of the model layers was calculated using the three-dimensional geometric depth of the layers and reflects their three-dimensional structure.

3. Experiments

We performed three series of 2-year experiments with different SSTs (Table 2). In each series we conducted five experiments with aerosols and five experiments without aerosols. The experiments were restarted with different initial conditions (same for corresponding experiments with and without aerosols). The restart conditions were chosen arbitrarily from the standard ECHAM4 reference experiments, thus providing five statistically independent realizations for each case. We evaluated the results by averaging the meteorological fields over the ensembles and calculating the statistical significance of the signals using the local *t*-test.

For the first series of experiments (marked by letter C in Table 2), we used climatological SSTs based on the 15-year reference period of 1979-1993. In the second series (marked by letter O in Table 2) the observed actual El Niño SSTs of 1991-1993 were used. In the third series (marked by letter L in Table 2) the La Niña SSTs of 1984-1986 were used as boundary conditions.

4. Observations

We choose air surface temperature to characterize the climate effects and geopotential heights to analyze the circulation response. For the surface air temperature, we used the gridded data set from *Jones and Briffa* [1992] (updated in 1994), worldwide station data, obtained from the Seewetteramt Hamburg for the years 1991-1993, and the gridded reanalysis data from the National Centers for Environmental Prediction (NCEP) [*Kalnay et al.*, 1996]. Original station data provide more detail than gridded data in regions with high station density.

For the free atmosphere, globally homogeneous data are available from space platforms. Measurements with the microwave sounding unit (MSU) give representative values of the vertically averaged temperature in the lower troposphere and the lower stratosphere [*Christy et al.*, 1995]. Because of vertical averaging of the lower tropospheric temperature in

Table 2. Labels for General Circulation Model Runs, Based on Boundary Conditions.

	Climatological SST	Observed SST (El Niño)	Observed SST (La Niña)
No aerosol forcing	C	O	L
With aerosol forcing	AC	AO	AL

SST, sea surface temperature.

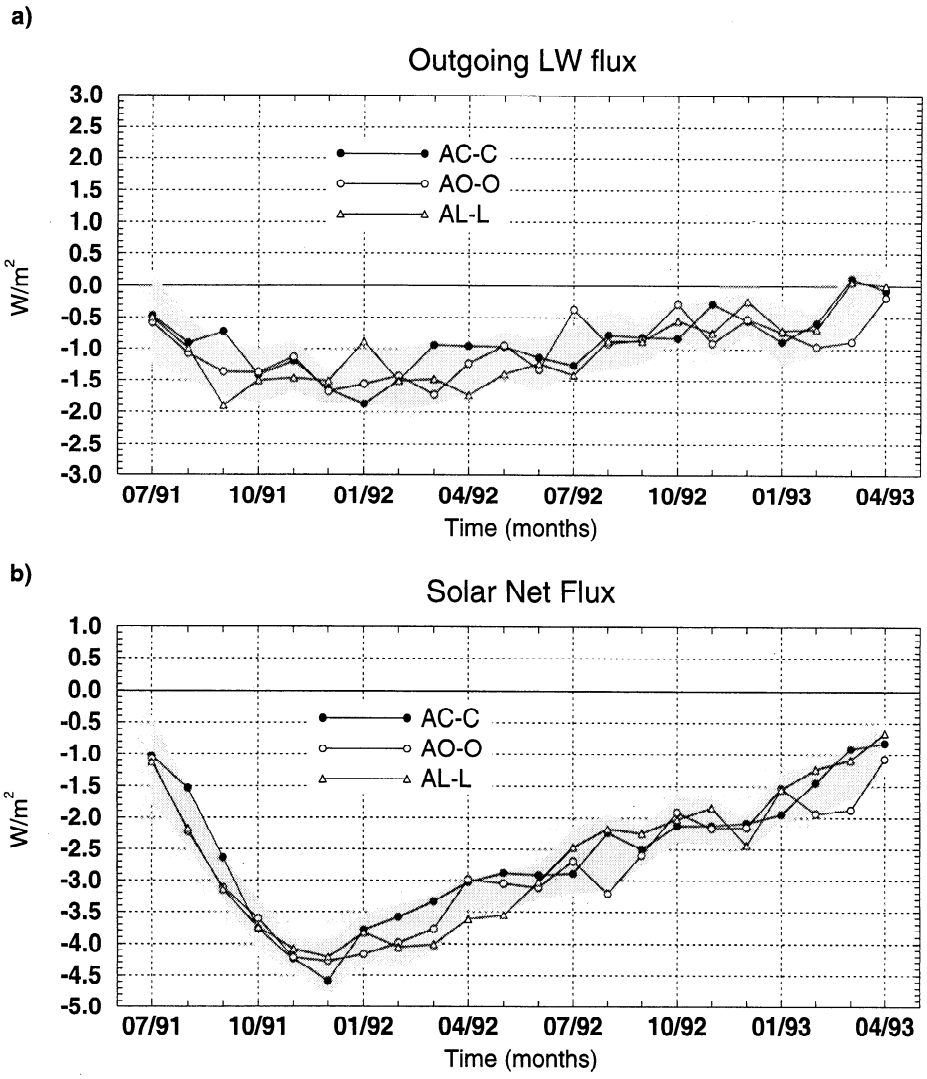

Figure 1. Global average simulated (a) longwave (LW) and (b) shortwave (SW) net flux anomalies at the top of the atmosphere caused by Pinatubo aerosols for different sea surface temperatures in AC, AO, and AL runs with respect to C, O, and L runs. The shaded area shows ±1 standard deviation.

the channel 2R observations [*Stendel and Bengtsson,* 1997], however, there are some differences in the anomaly structure of the temperature between MSU and surface air temperatures.

The NCEP data assimilation product [*Kalnay et al.*, 1996] is available for the last 30 years as a homogeneous global data set. It provides necessary information about atmospheric dynamics not available from the direct observations. To estimate the QBO effect, we also used wind data from *Naujokat* [1986] (updated in 1994).

For the lower stratosphere we also analyzed the radiosonde observations from the stratospheric group at the Free University of Berlin (FUB) [*Pawson et al.*, 1993]. These data were also used for the investigation of the connection between the lower stratospheric circulation and the tropospheric circulation by *Perlwitz and Graf* [1995]. The FUB group provides the geopotential heights and temperatures at 50 and 30 hPa. We found that NCEP reanalysis fields are in good agreement with the FUB data; therefore we present here only results using the NCEP product. For the stratosphere, we use the geopotential height at 50 hPa and temperature at 70 hPa.

To examine circulation effects in the troposphere, we chose the geopotential height at the 500 hPa layer and the temperature at the 850 hPa layer. We analyzed NCEP reanalysis data and MSU channels 4 and 2R. We found that temperature anomalies from both data sets agree well. Using NCEP reanalysis data we computed the climatology and statistics of free atmosphere for the period from January 1968 until June 1997.

5. Tropospheric Climate Response: Summer Cooling and Winter Warming

As we investigate the interactive response of climate system to aerosol radiative forcing, it is important to distinguish between forcing and response. The aerosol radiative forcing [*Stenchikov et al.*, 1998] is defined as the difference of the radiative fluxes at the surface and the heating rates in the atmosphere with and without aerosols,

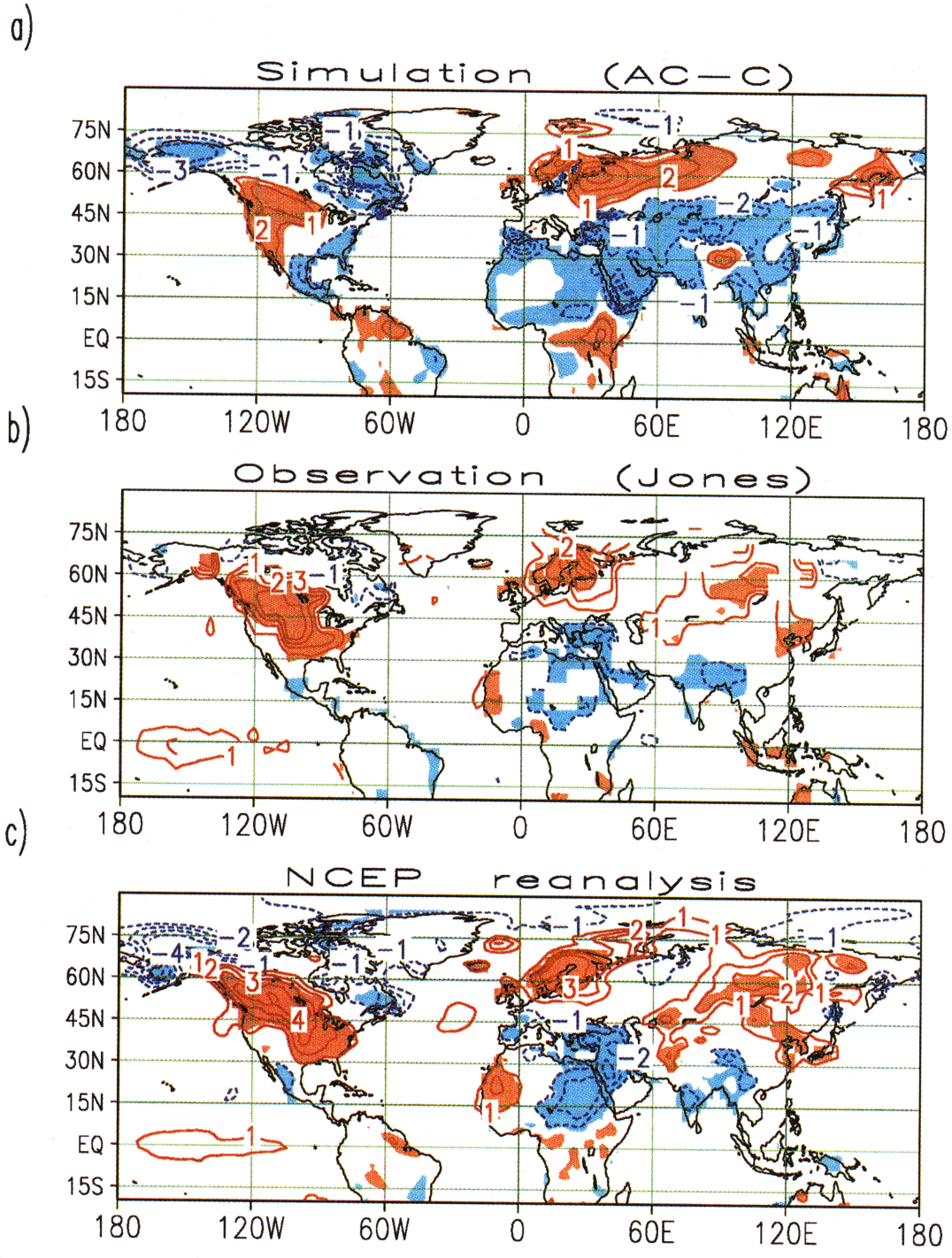

Plate 1. Anomalies of the surface air temperature (kelvins) in the winter (December-January-February) 1991-1992: (a) simulated in the run with climatological SST (shading corresponds to 10% confidence level), (b) calculated from National Centers for Environmental Prediction (NCEP) reanalysis data (shading corresponds to anomalies larger than one standard deviation), and (c) Calculated from observations [*Jones and Briffa*, 1992]. Simulated anomalies are calculated with respect to the ensemble runs without aerosol. Observed anomalies are calculated with respect to a 15-year average over the Atmospheric Model Intercomparison Project (AMIP) time period 1979-1993. Red color corresponds to positive anomalies and blue corresponds to negative.

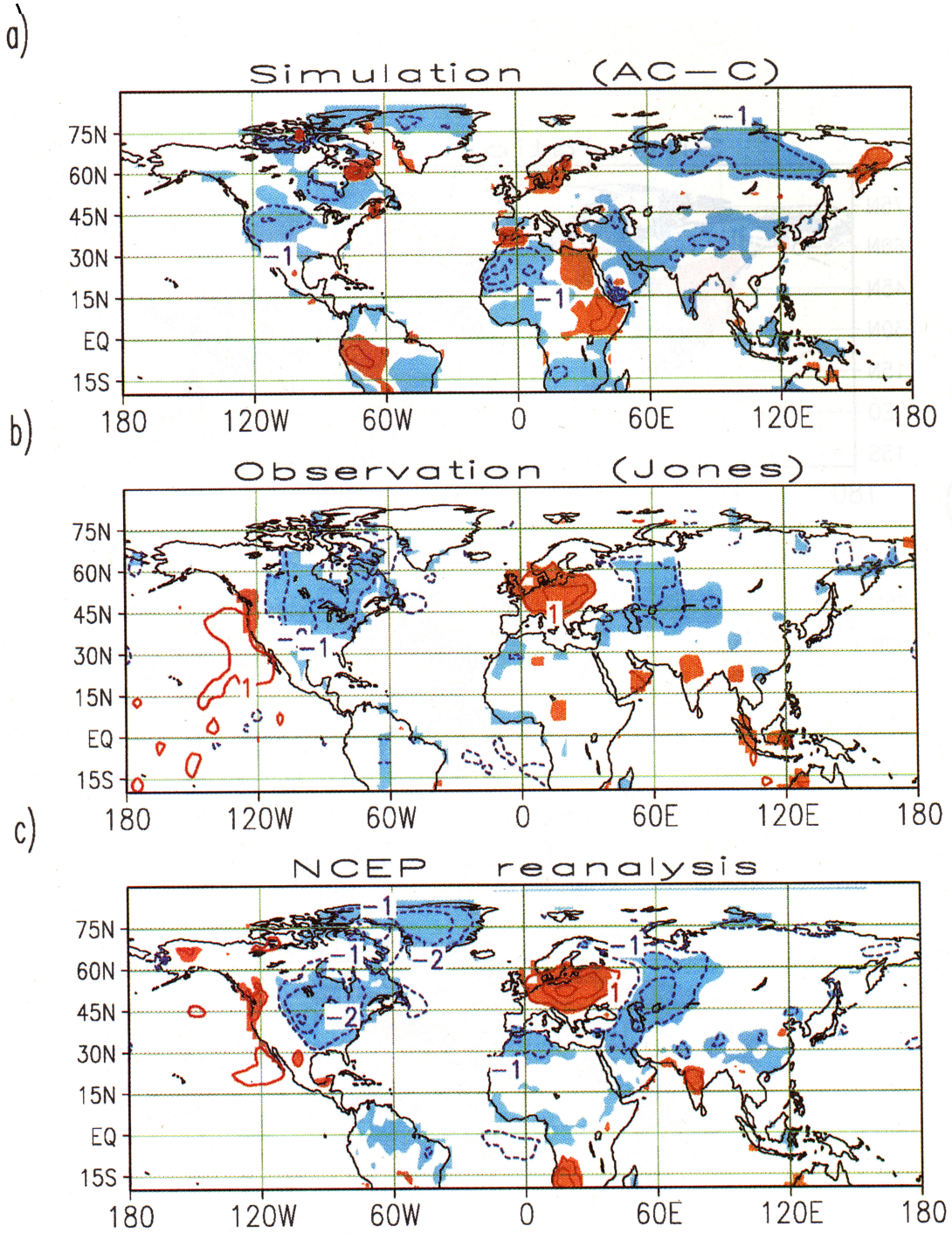

Plate 2. Same as Plate 1 but for summer (June-July-August) 1992.

evaluated on the same meteorological fields with no response to the aerosols. *Stenchikov et al.* [1998] showed that forcing is not sensitive to interannual variations of meteorology. They also pointed out that the "observed forcing" (we call it forcing with response) incorporates climate response, because radiative fluxes with and without aerosols are measured on different meteorological fields. Therefore we evaluated forcing with response to compare it with observations.

The change of the radiative fluxes at the top of the atmosphere characterizes the change of energy input into the whole climate system (Figure 1). The global average radiation balance correlates well with the evolution of the aerosol optical depth, and the differences between all three experiments are substantially smaller than the forcing itself. The net solar SW flux reduction is not compensated by LW aerosol absorption, making the total forcing negative. In the first winter after the eruption, the reduction of the solar energy reaches its largest value of more than 4 W/m^2. At the same time the decrease of the outgoing longwave radiation is the largest in January (1.5 W/m^2). The total net effect at the

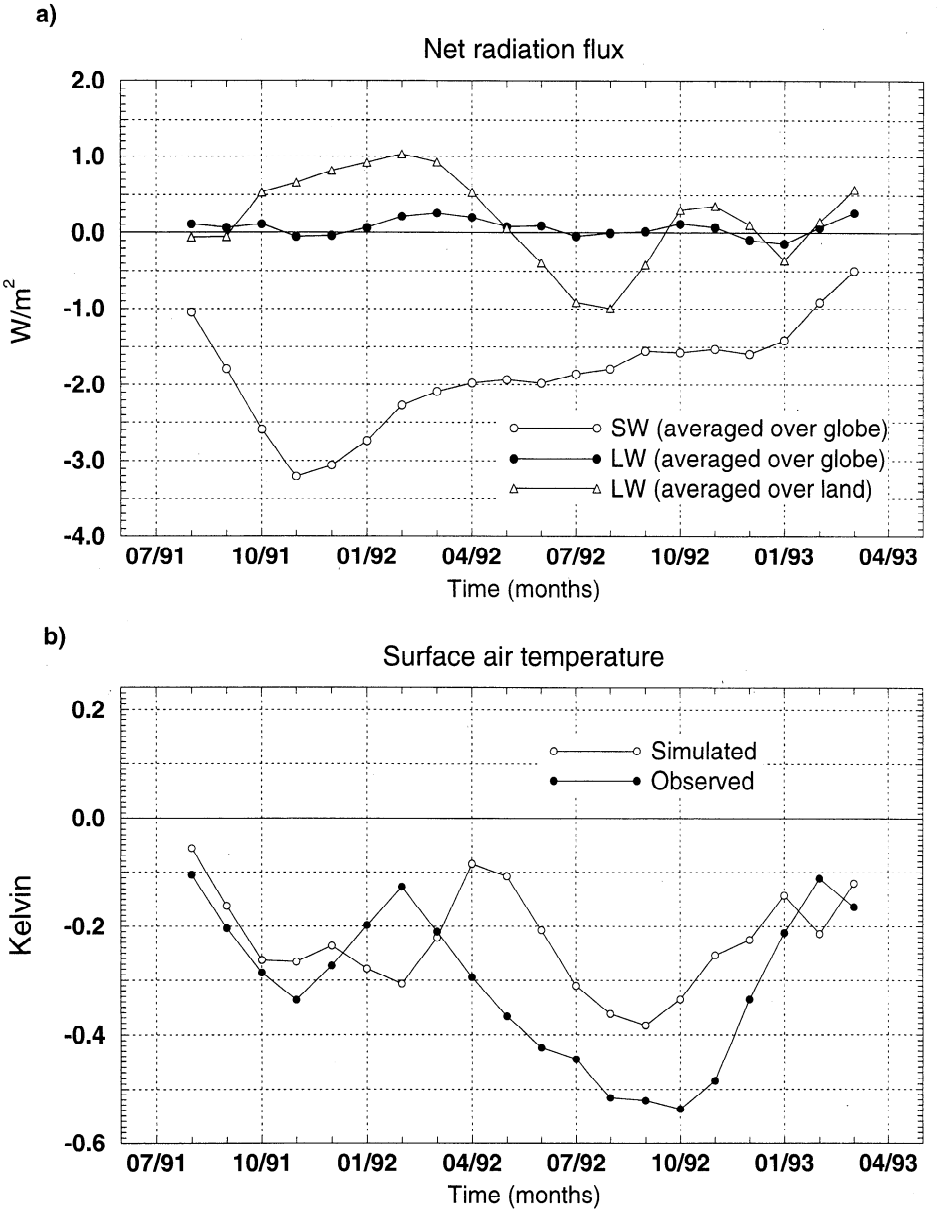

Figure 2. (a) The SW and LW net flux anomalies at the surface simulated in the experiment with climatological sea surface temperature (SST) (run AC – run C), averaged over the entire globe (SW and LW) and over land only (LW). (b) The surface air temperature anomaly from the run with climatological SST (averaged over land) and calculated from observations for the period 1950-1979 (averaged globally) [*Jones and Briffa*, 1992]. All curves are calculated as 3-month running averages.

top of the model is largest in December 1991, when it reaches a little more than -2.5 W/m^2. This figure agrees well with observations by *Russell et al.* [1993]. *Minnis et al.* [1993] found, using Earth Radiation Budget Experiment (ERBE) data, that the SW+LW net flux anomaly at the top of the atmosphere caused by the Pinatubo aerosol (forcing with response in our definition) equals -2.7±1 W/m^2.

Figure 2a shows the anomalies of net surface fluxes, and Figure 2b shows the surface air temperature anomalies in the observations and in the experiment with climatological SST (run AC – run C). The changes of SW and LW radiation at the surface were averaged over the whole globe. The LW and temperature were also averaged over land only. Over the ocean, SST is fixed. Therefore the model only responds with changes of land surface temperature. We first discuss the experiment with climatological SST and later focus on the effects caused by colder (La Niña-type) and warmer (El Niño-type) SSTs.

The global average (Figure 2a) solar net flux at the surface changes because of stratospheric aerosols by almost -3 W/m^2, with the maximum in the early winter of 1991-1992. After December 1991, the optical thickness of the aerosol decreases and the solar net flux anomalies become smaller. The flux reduction over the ocean would tend to decrease the ocean temperature, but these effects are not allowed in the experiment with climatological SST and are prescribed in the experiment with observed SST. Although the changes of ocean temperature because of radiative forcing would be

small, this simplification causes a decrease in the simulated cooling. The global average anomaly of LW flux at the surface over the ocean vanishes because of the fixed SST. The LW flux anomaly over land is positive during winter and negative during summer because of summer cooling and winter warming effects.

The simulated global cooling in summer (Figure 2b) is in good agreement with the observations. The amplitude of the anomaly reaches about 80% of the observed values partly because of the prescribed ocean. In winter, the amplitude of the temperature anomaly decreases in the experiment and in the observations because of the winter warming effect in the NH. This effect is caused not by direct radiative cooling, but by changes in the circulation. We discuss this in more detail in section 7, including the delay in winter warming as compared with the observations.

Plate 1 shows the simulated (run AC – run C) and observed pattern of surface air temperature anomalies in the first winter after the Pinatubo eruption. The observed temperature anomaly patterns are very similar to the mean anomaly calculated for a series of volcanic eruptions [*Robock and Mao*, 1992]. Over North America and Europe, we found large regions with similar simulated and observed anomalies. The cooling over the eastern Mediterranean is also well reproduced. Over Asia southward of 50°N, the model produces cooling, which we do not see in the observations, where positive temperature anomalies over Siberia dominate.

Regions with negative temperature anomalies in the summer of 1992 are simulated in the AC run over large parts of North America, North Africa, and Asia (Plate 2). The direct aerosol effect on radiation significantly reduces regional temperature by about 1 K in the simulations, agreeing well with observations over North America and North Africa, but not with the observed warming in South America and Europe or the warming over Africa. The overall simulated summer cooling effect is slightly weaker than observed (see Figure 2). Since the detailed temperature pattern in the summer depends on the particular atmospheric circulation pattern, which depends on chaotic weather variations and SST forcing, we do not expect an exact agreement between our simulations and observations. Only in the NH winter is the dynamical pattern strongly forced by volcanic aerosols.

We calculated the MSU channel 2R anomaly signal with temperature fields simulated in the AC and C runs and the NCEP reanalysis (with respect to 1986-1990 reference period) using the weighting function for channel 2R from *Stendel and Bengtsson* [1997] and compared them with the latest update of the actual MSU observations [*Christy et al.*, 1995], including the effects of satellite orbit degradation [*Wentz and Schabel*, 1998]. Although not all the features of the surface air temperature anomalies are well simulated, for the less noisy vertically integrated lower tropospheric temperature anomaly (Figure 3) the comparison with observations is fairly good. The MSU channel 2R measurements show cooling over China. The winter warming over the North Atlantic and adjacent regions, for all three panels with observations, reanalysis, and simulations, corresponds well to the winter warming pattern found after all major volcanic eruptions of the past century [*Robock and Mao*, 1992, 1995].

6. Stratospheric Thermal Response: Effects of Aerosols, QBO, and Ozone

While tropospheric changes are most commonly associated with a volcanic climate signal, significant heating of the lower stratosphere because of aerosol LW and solar near-IR absorption is another important effect. This stratospheric heating modulates the stratospheric circulation, which affects tropospheric large-scale wave patterns. The structure and evolution of heating rate anomalies because of volcanic aerosols were discussed by *Stenchikov et al.* [1998].

Figure 4 shows a Hovmoeller diagram of the zonal averaged (observed and simulated in the run with climatological SST) lower stratospheric temperature anomaly at the 70-hPa level. In the simulation, the temperature anomaly is 2 times larger than observed in the first winter following the eruption. In the second winter, the simulated anomalies are the same or even lower than the observations. These discrepancies between the calculated aerosol effect and observations are caused by the quasi-biennial oscillation (QBO) and ozone depletion, which contribute to the observed response.

Angell [1997b] showed that during the QBO easterly phase, stratospheric temperature decreases in the tropics by about 1 K. This effect was well observed for the 1992 easterly phase of QBO. In 1993, a west phase of the QBO warmed the tropical stratosphere, in addition to aerosol LW and near-IR absorption. Therefore the calculated signal is too warm for 1992 but closer to the observed anomaly for 1993 (Figures 4a and 4b).

Figure 5a shows the observed temperature anomalies at the 70-hPa level based on NCEP reanalysis data (with respect to a 1968-1997 climatology) averaged between 10°S and 10°N, which includes the QBO effect, and the corresponding simulated anomalies (with respect to the C run) in the AC run. To estimate the QBO effect on the simulated anomalies, we calculated a mean QBO temperature cycle. During the period of available observations (1968-1997), there were 10 QBO cycles. Two of them were affected by the volcanic eruptions of El Chichón (1982) and Pinatubo (1991) and therefore were not included in averaging. We centered a QBO cycle on the month when the zonal wind in the tropics at 50 hPa changed from east to west. Using this criterion, we chose May 1971, March 1973, July 1975, December 1977, May 1980, October 1982 (not used in the averaging), March 1985, September 1987, May 1990, and December 1992 (not used in the averaging). We calculated the mean stratospheric temperature anomalies for 49 months beginning 24 months before the above defined month and ending 24 months after it for all the above cycles. To estimate the QBO effect on stratosphere temperature after the Pinatubo eruption, we superposed these mean QBO cycle temperature anomalies on the NCEP climatology. In Figure 5a we centered the calculated mean QBO cycle on December 1992. The shaded area in Figure 5a indicates the QBO-corrected stratospheric temperature anomaly. During 1992, the observed lower tropical stratosphere temperature anomaly calculated with respect to the climatology underestimates the aerosol stratospheric heating by almost 1 K. This explains part of the discrepancy between the computed and observed stratospheric heating. The rest of the discrepancy is related to ozone depletion.

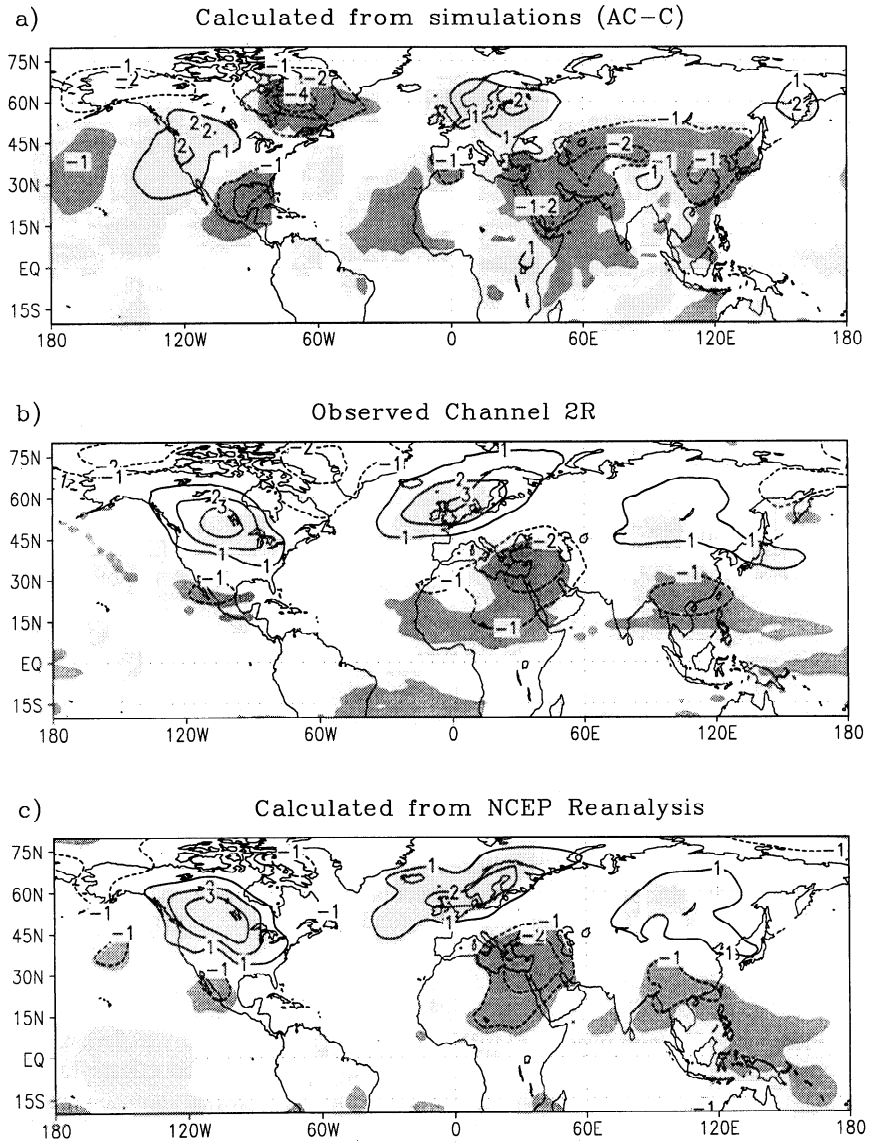

Figure 3. Lower troposphere temperature anomalies for Northern Hemisphere winter 1991-1992: (a) difference between the two general circulation model (GCM) ensembles with and without stratospheric aerosols (run AC – run C) vertically integrated with the channel 2R weighting function [*Stendel and Bengtsson*, 1997]; (b) observed anomalies from channel 2R of the microwave sounding unit (MSU) satellite observations, representative for the lower troposphere; and (c) vertically integrated temperature anomalies from NCEP reanalysis [*Kalnay et al.*, 1996] using channel 2R weighting function to synthesize the MSU signal. All anomalies are calculated with respect to the 1986-1990 reference period. Contour interval is 1 K. In all panels, shading corresponds to 20% confidence level, with positive values having a lighter shading.

Volcanic aerosols produce ozone chemical loss in the middle latitudes because of the intensification of heterogeneous reactions. This process has a characteristic time of several months. Therefore the radiative effect of ozone depletion in midlatitudes can be detected only approximately 6 months after an eruption [*Akiyoshi,* 1997]. In the tropics, however, where the thermal effect is the largest, the ozone mixing ratio decreases because of lifting of tropospheric air into the stratosphere [*Kinne et al.*, 1992]. Therefore reduction of ozone and of the resulting UV absorption affects temperatures in the tropics during the entire time after the eruption. In this particular experiment, we do not account interactively for the ozone depletion effect on stratospheric temperature, but estimate it off-line. We performed one winter experiment with stratospheric aerosols, climatological SSTs, and prescribed ozone reduction. We introduced ozone depletion between 40 and 110 hPa in the model with the total column ozone reduction from *Angell* [1997a]. In this layer, the aerosol heating and the corresponding effects on ozone are the largest. The total ozone reduction was specified to be 2%

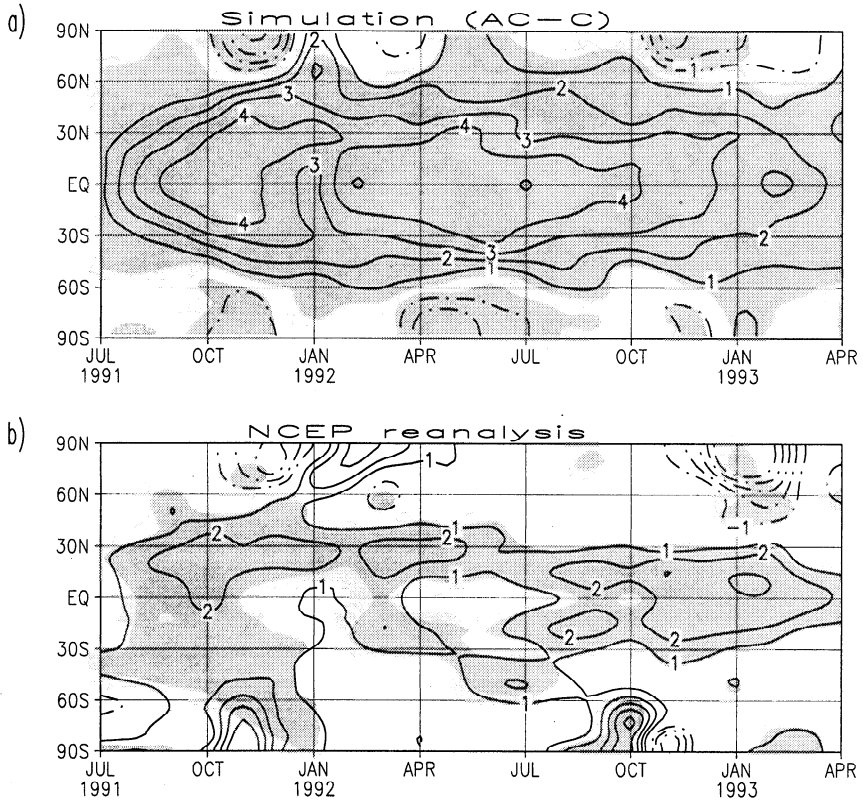

Figure 4. Hovmoeller diagram of the zonal averaged anomalies (kelvins) of lower stratosphere temperature at the 70-hPa level caused by Pinatubo aerosols: (a) simulated in the run with climatological SST (run AC – run C), (the shading corresponds to 10% confidence level) and (b) calculated from NCEP reanalysis with respect to the 1968-1997 climatology [*Kalnay et al.*, 1996] (the shading corresponds to anomalies larger than one standard deviation).

in the Southern Hemisphere and 7% northward of 40°N [*Angell*, 1997a]. Between the equator and 40°N, it changed linearly from 2% to 7%. With these assumptions, the calculated ozone reduction in the aerosol layer reached 20%. *Grant et al.* [1992] and *Grant* [1996] observed an ozone reduction in the tropics of approximately 20% in the aerosol layer between 16 and 28 km.

Figure 5b shows the global averaged observed temperature anomaly at the 70-hPa layer, compared with the average simulated response in the AC run and the off-line estimate of the ozone effect. The direct heating due to the aerosols reaches about 3 K six months after the eruption. The ozone cooling reduces the stratospheric temperature response by approximately 1 K. Combining the QBO and ozone effects, we see that accounting for ozone depletion decreases the simulated anomaly by 1 K (Figure 5b) and accounting for the QBO cycle increases the observed anomaly by 1 K (Figure 5a). This completely explains the 2-K discrepancy between observed and simulated temperature anomalies in Figure 5b.

The previous analysis shows that it is important to account for the QBO and ozone depletion effects because they significantly affect the amplitude of lower stratospheric heating. Their related direct effects in the troposphere are fairly small, but they can affect the troposphere indirectly by forcing dynamical processes in the troposphere. We do not have enough information to include these QBO and ozone depletion effects in our simulations at the present time. The comparison of all three effects (aerosols, QBO, and ozone depletion) shows that the aerosols produce the strongest effect, so at this time we compare the climate response to the aerosol-only forcing with the observations. The favorable comparison of the simulated and observed fields in Plates 1 and 2 and Figure 3 supports this point.

The climate response consists of fairly robust direct radiative tropospheric cooling and stratospheric heating, and winter warming which is caused indirectly by changes in circulation. The dynamical effect is difficult to simulate with current state-of-the-art GCMs and incomplete formulation of all components of the forcing, as discussed above. To simulate winter warming, we conducted an ensemble of calculations with different SSTs.

Even with perfect stratospheric forcing, we would not expect perfect agreement with observations. To achieve that, we would need a model that also responded perfectly to SST anomalies, and we would require that chaotic weather and circulation variations be so small that the aerosol external forcing would dominate the winter circulation. We attempt to address this last problem by conducting an ensemble of simulations, but the real world only presents us with one member of its ensemble, so even a perfect model with a large ensemble would not agree perfectly with the observations for any specific year. That is why it is not surprising that our

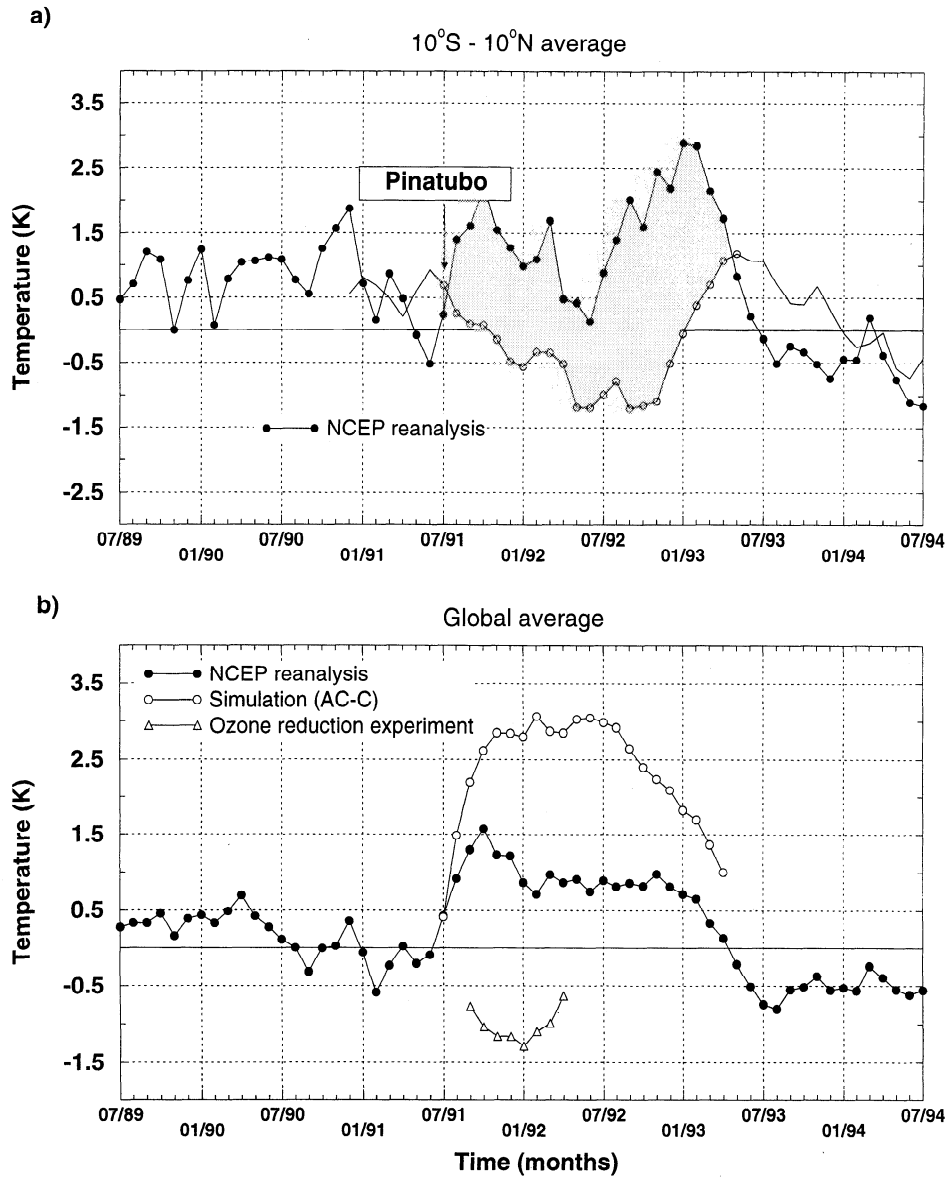

Figure 5. (a) Lower stratosphere temperature anomalies (kelvins) at 70 hPa calculated from NCEP reanalysis with respect to 1968-1997 climatology and averaged for 10°S-10°N latitudes, and the quasi-biennial oscillation (QBO) temperature cycle with respect to the same climatology and averaged in the same latitude band. The shaded area is the Pinatubo signal after accounting for the QBO effect. (b) Global averaged temperature anomalies (kelvins) calculated from the NCEP reanalysis with respect to 1968-1997 climatology, simulated in the run with climatological SST (run AC – run C), and caused by the prescribed observed ozone reduction.

simulated response is in better agreement with the observed response averaged over a series of eruptions [*Robock and Mao,* 1995].

7. Stratosphere-Troposphere Coupling: Dynamic Response and Sensitivity to SST

The tropospheric warming in the northern winter is the result of an atmospheric dynamical response that produces changed advective patterns. Aerosol heating in the tropical lower stratosphere increases the meridional temperature gradient, which forces the zonal circulation and produces a stronger polar vortex. The stronger vortex prevents the advection of energy to the pole by eddy fluxes in the stratosphere [*Kodera et al.,* 1991; *Kodera,* 1994; *Boville,* 1983] and the temperature of the lower stratosphere over the pole decreases, as observed by *Angell* [1997b]. The polar cooling itself intensifies the lower stratospheric vortex (Figure 6). This positive feedback mechanism helps to keep the vortex strong. In the experiments with climatological SST (AC and C runs), we see cooling of the polar lower stratosphere in both winters after the eruption (Figure 4) and enhancing of the NAO circulation pattern in troposphere (Figures 8a and 8e for the model and Figures 8d and 8h for observations). The

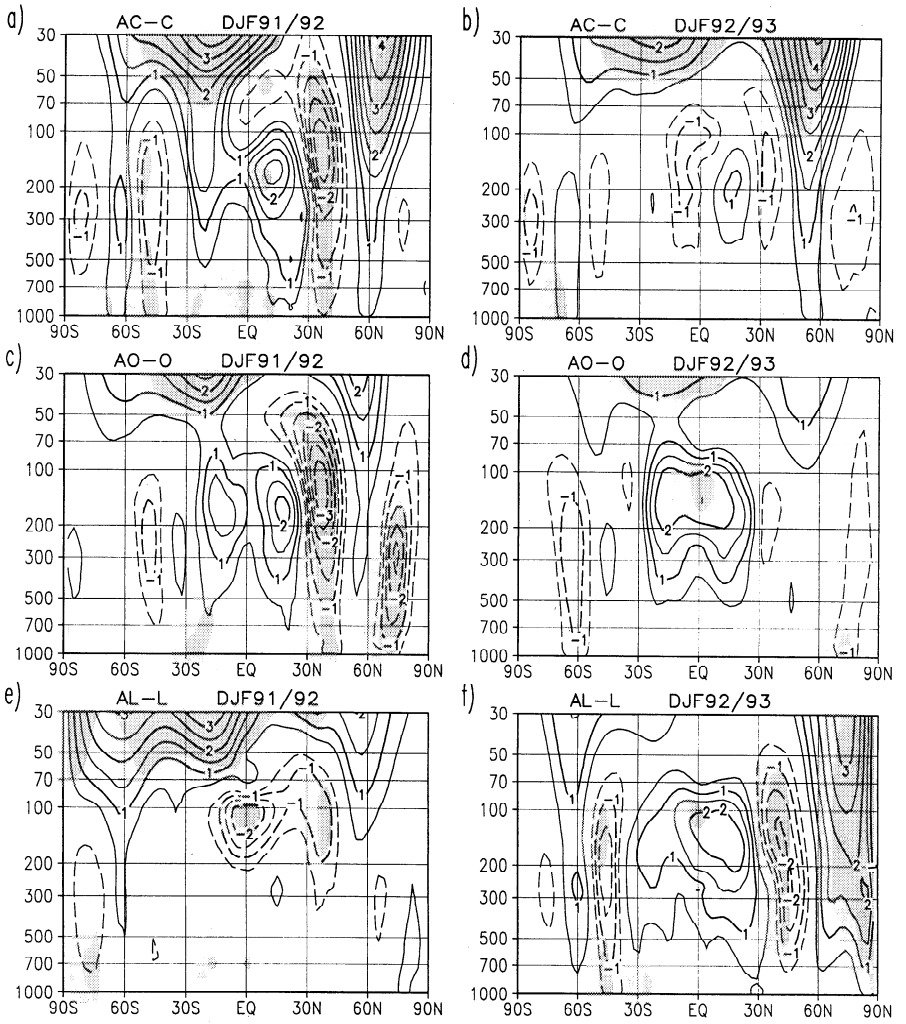

Figure 6. Zonal averaged zonal wind anomalies (m/s): simulated in the experiment with climatological SST (run AC – run C) for the winters of (a) 1991-1992 and (b) 1992-1993; simulated in the experiment with observed warm SST (run AO – run O) for the winters of (c) 1991-1992 and (d) 1992-1993; simulated in the experiment with cold SST (run AL –run L) for the winters of (e) 1991-1992 and (f) 1992-1993 (the shading corresponds to anomalies larger than one standard deviation).

simulated vortex anomalies, however, are not as strong and stable as in the observations because the model already has a too strong and long-lasting polar vortex in the climatological run without aerosols. The simulated anomaly becomes weaker later in the winter and restores in the spring, producing late winter warming in April (Figure 2). The amplitude of the NAO pattern follows the intensity of the polar vortex.

To study the dynamical effects, we address two main questions: What are the dynamical processes which affect the lower stratospheric circulation in the high northern latitudes, and what are the changes in the tropospheric midlatitude winter circulation? We focus on the NH winters, compare the simulated response with observations, and look specifically at its sensitivity to SSTs. *Kodera* [1994] and *Graf et al.* [1994] proposed that an increase of the meridional temperature gradient in the lower stratosphere because of aerosol radiative heating at low latitudes produces dynamical forcing. In our experiment with only the aerosol effect (without QBO and ozone depletion), this gradient forcing is overestimated in the first winter and probably is more realistic in the second winter.

7.1. The Stratospheric Circulation Response

Figure 6 shows the changes of the zonally averaged zonal circulation in the winters of 1991-1992 and 1992-1993. In the AC run, we get a strong increase of the North Pole vortex in the winter. The zonally averaged zonal wind at 60°N is 4 m/s stronger in the AC run than in the C run. The shading shows the anomalies larger than one standard deviation, calculated from the 15-year AMIP run with climatological SST. Aerosols in combination with the observed warm SST (run AO – run O) lead to a significantly weaker perturbation of the polar vortex in both winters. In the run with cold SST (run AL – run L) the vortex is weaker in the first winter but in the second winter is increased as much as in the AC run. The circulation response is sensitive to SSTs, because SST affects the general circulation fields, and the wave structure in the troposphere and the stratosphere-troposphere interactions depend significantly on these factors.

To look at the changes in the wave structure in the lower stratosphere we choose the 50-hPa layer height anomaly in all the experiments (Figure 7). We compare the simulated re-

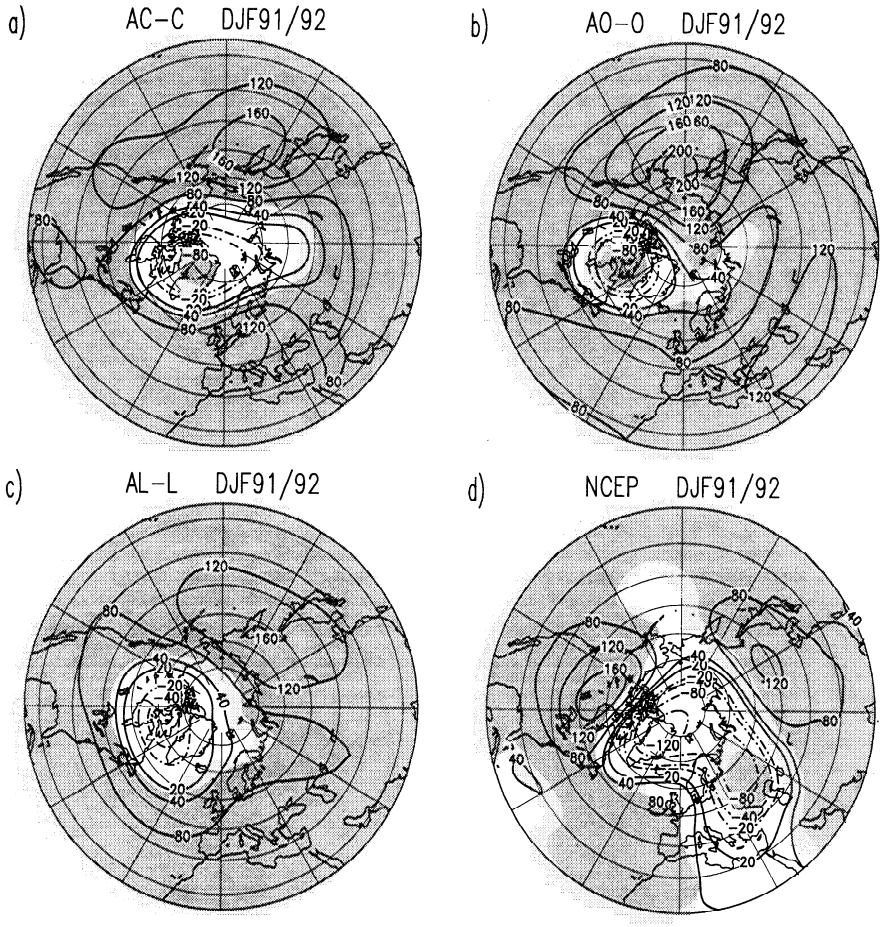

Figure 7. Seasonal averaged anomalies of geopotential height (meters) at 50 hPa: (a) simulated in the experiment with climatological SST (run AC – run C) for the winter 1991-1992; (b) simulated in the experiment with observed warm SST (run AO – run O) for the winter 1991-1992; (c) simulated in the experiment with cold SST (run AL – run L) for the winter 1991-1992; (d) calculated from the NCEP reanalysis data for the winter 1991-1992 with respect to the 1968-1997 climatology [*Kalnay et al.*, 1996]; (e) simulated in the experiment with climatological SST (run AC – run C) for the winter 1992-1993; (f) simulated in the experiment with observed warm SST (run AO – run O) for the winter 1992-1993; (g) simulated in the experiment with cold SST (run AL – run L) for the winter 1992-1993; and (h) calculated from the NCEP reanalysis data for the winter 1992-1993 with respect to the 1968-1997 climatology [*Kalnay et al.*, 1996]. The shading for Figures 7a, 7b, and 7c corresponds to a 10% confidence level. The shading for NCEP data (Figure 7d) corresponds to anomalies larger than one standard deviation.

sponse with the NCEP reanalysis. For 1991-1992, the simulated geopotential field is characterized by a negative anomaly near the pole, with the center located over the Labrador Sea and Baffin Bay. In the first winter, the location is independent of SST (Figures 7a-7c). In the second winter, all experiments show a different pattern over the pole (Figures 7e-7g). Only the experiment with climatological SST reproduces the structure of the first winter and exceeds a significance level of 90%. In the observations in both northern winters following the Pinatubo eruption the polar vortex is stronger than normal. In the 1992-1993 winter, the perturbation is symmetric over the pole and stronger than in the 1991-1992 winter. El Niño-Southern Oscillation (ENSO) and the QBO, which was in its easterly phase, affected the circulation in 1991-1992 and reduced the strength of the polar vortex.

In all runs, the intensity of the stratospheric dynamic response is underestimated in comparison with observations. The geopotential height anomaly near the pole is much smaller than observed, and its center is shifted toward Greenland for all SSTs. The polar vortex simulated in the AC run looks closest to the observed one, but the wave amplitudes and eddy flux are suppressed in the simulations (Figure 7). Therefore the positive feedback with polar temperature is weaker. This causes a weaker dynamic response in the lower stratosphere than in the observations.

The simulated thermal response to the volcanic aerosol in the tropical lower stratosphere is independent of the SSTs. The temperature increases there by about 3-4 K. The response over the polar region during the winter is much more variable. The position and the strength of the vortex anomaly are different in the experiments with different SSTs, which shows the importance of the tropospheric influence. Therefore the effect of the stratosphere on the tropospheric circulation is quite uncertain in the high latitudes. The mechanism of stratosphere-troposphere interaction discussed by *Kodera et al.* [1991], *Kodera* [1994], *Graf et al.* [1994], and *Perlwitz and Graf* [1995] implies that change of the mean circulation in the lower stratosphere caused by a stronger equator-pole temperature gradient affects the tropospheric wave structure, because of wave reflection and mean flow-

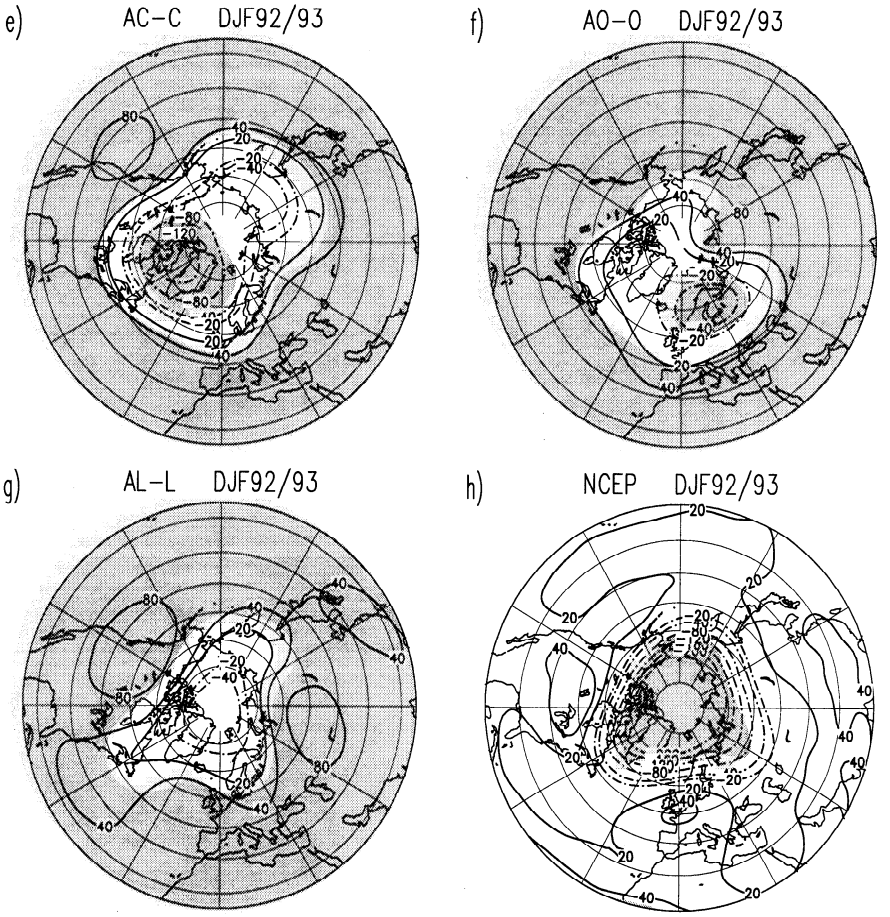

Figure 7. (continued)

wave interaction. The enhanced polar vortex modifies the direction of the planetary wave energy flux [*Boville*, 1983]. In the case of a stronger vortex, more wave energy goes back to the troposphere and forms stationary wave patterns like the NAO [*Kodera et al.*, 1991; *Kodera*, 1994; *Graf et al.*, 1994]. Our simulations show that the effect on the troposphere could be different for similar regimes of lower stratosphere heating in experiments with different SSTs. This means that the polar vortex itself is affected by the tropospheric circulation. Therefore a strengthened stratospheric latitudinal temperature gradient is not the only important factor for tropospheric changes.

7.2. Tropospheric Circulation Response

To look at the changes in the wave structure in the troposphere, we choose the 500-hPa layer height anomaly in all the experiments (Figure 8) and compare them with the observations. In the observations the anomaly structure in both winters is similar at the pole and in the Eastern Hemisphere. Between 30°E and 60°E and over the North Pole the geopotential height anomaly is negative. Over northwest Europe the geopotential height anomaly is positive and centered over Great Britain. In the western part of the hemisphere in the 1991-1992 winter, the geopotential height anomaly near the Aleutian low over the northeast Pacific is negative, affected by the warm Pacific at this time. This anomaly in the second winter, 1992-1993, shifts toward the west coast of North America. The positive geopotential height anomaly over North America is larger in the first winter than in the second. In both winters the anomaly structure is characterized by a low over Greenland, a high over Great Britain, and a trough over the Urals.

In the simulations with the same SSTs we get strong differences in circulation between the first and second winters. The circulation is different as well for the same winters in the experiments with different SSTs. A positive geopotential height anomaly over Europe appears only in the first winter in the experiment with climatological SST. In this experiment the structure of the anomalies over Greenland and North America also fits the observations. In the first winter in the AO run, the positive anomaly over the Atlantic centered at 45°W and 50°N is strongest. A similar circulation pattern also forms in the AC run in the second winter. In the AL run, the positive geopotential height anomaly over western Europe is simulated, but the negative anomaly over Greenland is missing.

The vertical structure of the response pattern shows that the model response is more barotropic than in the observations [*Perlwitz and Graf*, 1995]. Only large-scale tropospheric waves can interact with the stratosphere. The mechanism of interaction is nonlinear and depends on the intensity of the westerlies [*Boville*, 1983]. The response is sensitive to the mean circulation and the wave structure in the troposphere and therefore to SST. Because of this high sensitivity and

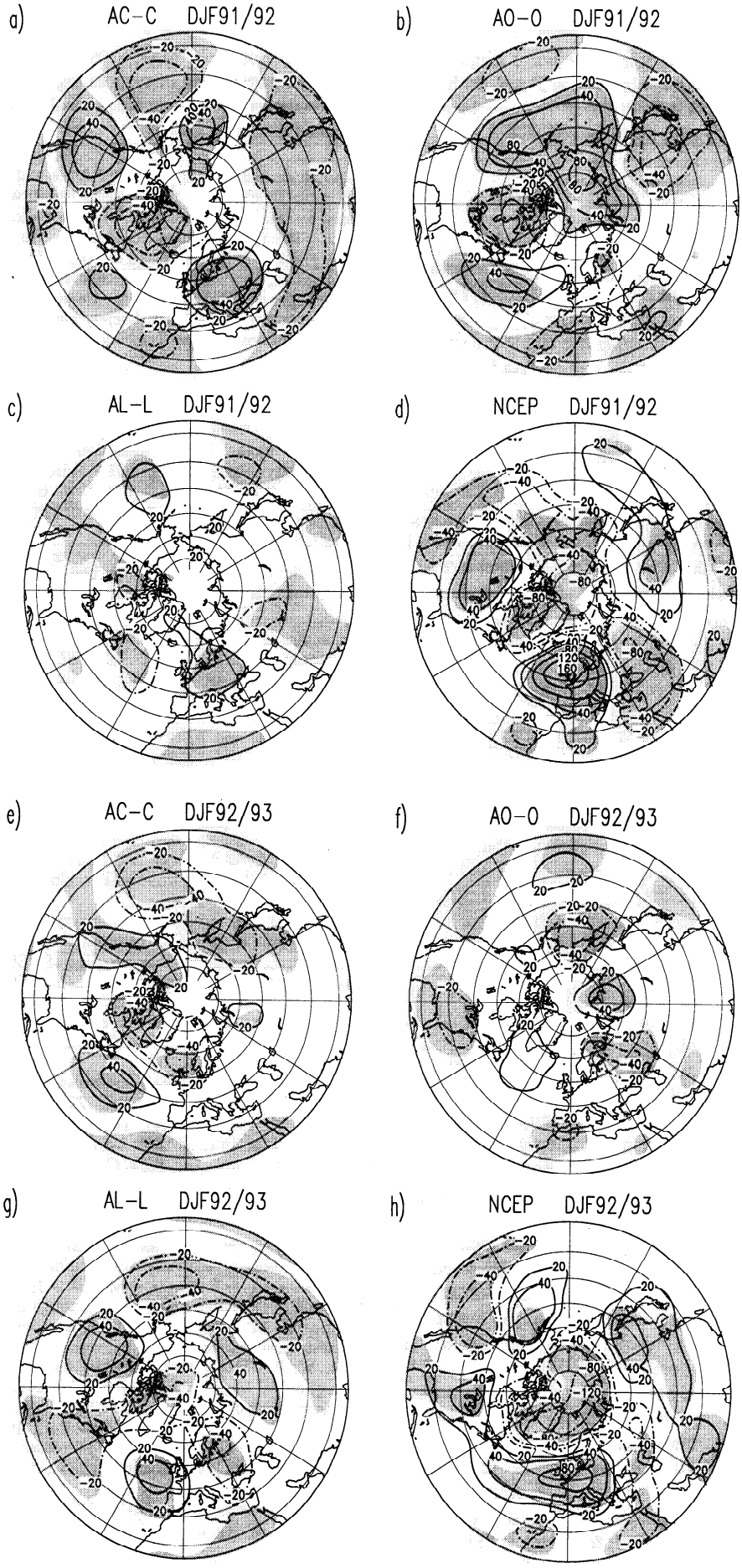

Figure 8. Same as in Figure 7, but for 500 hPa.

GCM deficiencies in the description of the wave structure in response to the SST variations in the AC run with the climatological SST, the "winter warming" pattern is more realistic than in the AO run with the observed SST.

8. Discussion and Conclusions

Using realistic aerosol characteristics, we simulated with ECHAM4 the climate response to the 1991 Pinatubo eruption, studied the climate response and its sensitivity to SSTs, and compared the results with observations. The change of solar radiative fluxes at the top of the atmosphere and at the surface are in good agreement with the ERBE and Mauna Loa observations. The amplitude of the global radiation response to stratospheric aerosols is independent of the SSTs. The stratospheric thermal response to aerosol forcing is in good agreement with observations after accounting for the effects of QBO and ozone depletion. The ozone depletion in the aerosol layer reduces the stratospheric heating by 30%. The QBO masks the temperature response of the lower stratosphere by 1 K. The stratospheric thermal response is independent of SST.

Summer cooling is well reproduced in all the experiments. Winter warming patterns in January have a realistic structure but too weak an amplitude in the experiments with the climatological SST. The summer cooling is a direct effect of the aerosol radiative forcing, but the winter warming is a result of induced changes in the tropospheric circulation, caused by stratosphere-troposphere dynamical interaction.

The dynamical effect is difficult to simulate because of model deficiencies and incomplete formulation of forcing. We conducted an ensemble of calculations with different SSTs. The winter warming pattern is better simulated in the runs with climatological SST. The aerosol forcing and lower stratospheric thermal response are fairly stable with respect to the SSTs. The tropospheric climate response, however, is quite different, because of a high sensitivity of stratosphere-troposphere interaction to the background wave structure formed by SSTs. The worse results in the simulations with observed SSTs are because of too strong coupling in ECHAM4 between the model temperatures and tropical SSTs, probably because of the convective parameterization [*Roeckner et al.*, 1996b]. The inability of our model to respond to SST anomalies, however, is by no means unique [*Chen and van den Dool*, 1997]. The tropospheric thermal response is sensitive to SSTs, because the tropospheric Rossby waves are sensitive to the SSTs and play an important role in the stratosphere-troposphere dynamic interaction. The anomalies over North America are strongly connected to the increase of the baroclinic mode, which is simulated nearly as observed.

We have produced the best ever GCM simulation of the winter warming dynamical response of the climate system to volcanic aerosol forcing. The results are very similar to the actual observations for the winter of 1991-1992, which is surprising because the observed pattern depends not only on the volcanic forcing, but also on the El Niño and natural chaotic weather variations. On the basis of numerous previous observational and model studies we discuss the robust features of the stratospheric and tropospheric responses and suggest the most plausible explanations. This experiment is reported here to serve as a benchmark for attempts to improve climate model response to volcanic aerosol forcing. Such models must do a good job of describing the coupling of the dynamic stratosphere-troposphere interaction with the NAO circulation pattern and of responding to SST anomalies. We would be happy to provide the aerosol data set we used to any interested modeling groups.

Acknowledgments. We thank Phil Jones and John Christy for data used in the figures. The figures were drawn with GrADS software, created by Brian Doty, and the XVGR package, developed by Paul J. Turner. The work is supported by NSF grant ATM-9528201 and NASA grants NAGW-5227 and NAG-55161. Part of the work was performed during visits of G. Stenchikov and A. Robock to MPI, and of I. Kirchner and H.-F. Graf to the University of Maryland, partially supported by the Max-Planck-Society and the VW Foundation. The GCM simulations were performed under a grant from BMBF.

References

Akiyoshi, H., Development of a global 1-D chemically radiatively coupled model and introduction to the development of a chemically coupled general circulation model, *CGER Supercomput. Monogr. Rep. vol. 4*, 69 pp., Cent. for Global Environ. Res., Nat. Inst. for Environ. Stud., Environ. Agency of Jpn., Tokyo, 1997.

Angell, J. K., Estimated impact of Agung, El Chichón, and Pinatubo volcanic eruptions on global and regional total ozone after adjustment for the QBO, *Geophys. Res. Lett., 24*, 647-650, 1997a.

Angell, J. K., Stratospheric warming due to Agung, El Chichón, and Pinatubo taking into account the quasi-biennial oscillation, *J. Geophys. Res., 102*, 9,479-9,485, 1997b.

Boville, B. A., The influence of the polar night jet on the tropospheric circulation in a GCM, *J. Atmos. Sci., 41*, 1132-1142, 1983.

Charney, J. G., and P. G. Drazin, Propagation of planetary-scale disturbances from the lower into the upper atmosphere, *J. Geophys. Res., 66*, 83-109, 1961.

Chen, W. Y., and H. M. van den Dool, Asymmetric impact of tropical SST anomalies on atmospheric internal variability over the North Pacific, *J. Atmos. Sci., 54*, 725-740, 1997.

Christy J. R., R. W. Spencer, and R. T. McNider, Reducing noise in the MSU daily lower-tropospheric global temperature dataset, *J. Clim., 8*, 888-896, 1995.

Coffey, M. T., Observations of the impact of volcanic activity on stratospheric chemistry, *J. Geophys. Res., 101*, 6767-6780, 1996.

Crutzen, P. J., The possible importance of CSO for the sulfate layer of the stratosphere, *Geophys. Res. Lett., 3*, 73-76, 1976.

Deutsches Klimarechenzentrum, Modelbetreuungsgruppe, The ECHAM3 atmospheric general circulation model, *Rep. 6*, revision 2, 190 pp., Max-Planck-Inst. für Meteorol., Hamburg, Germany, 1993.

Gates, W. L., AMIP: The Atmospheric Model Intercomparison Project, *Bull. Am. Meteorol. Soc., 73*, 1962-1970, 1992.

Giorgetta, M., and M. Wild, The water vapor continuum and its representation in ECHAM4, MPI Rep. 162, 38 pp., Max-Planck-Inst. für Meteorol., Hamburg, Germany, 1995.

Graf, H.-F., I. Kirchner, A. Robock, and I. Schult, Pinatubo eruption winter climate effects: Model versus observations, *Clim. Dyn., 9*, 81-93, 1993.

Graf, H.-F., J. Perlwitz, and I. Kirchner, Northern hemisphere tropospheric mid-latitude circulation after violent volcanic eruptions, *Contrib. Atmos. Phys., 67*, 3-13, 1994.

Graf, H.-F., J. Feichter, and B. Langmann, Volcanic sulfur emission: Estimates of source strength and its contribution to the global sulfate distribution, *J. Geophys. Res., 102*, 10,727-10,738, 1997.

Grant, W. B., Tropical stratospheric ozone changes following the eruption of Mount Pinatubo, in *The Mount Pinatubo Eruption Effects on the Atmosphere and Climate, NATO ASI Ser.*, vol. I 42, pp. 161-175, Springer-Verlag, New York, 1996.

Grant, W. B., et al., Observations of reduced ozone concentration after the eruption of Mount Pinatubo, *Geophys. Res. Lett., 19*, 1109-1112, 1992.

Jones, P. D., and K. R. Briffa, Global surface air temperature variations during the twentieth century, *Holocene, 2*, 165-179, 1992.

Junge, C. E., C. W. Chagnon, and J. R. Manson, Stratospheric aerosol, *J. Meteorol., 18*, 81-108, 1961.

Kalnay, E., et al., The NCEP/NCAR 40-year reanalysis project, *Bull. Am. Meteorol. Soc.*, *77*, 437-471, 1996.

Kinne, S., O. B. Toon, and M. J. Prather, Buffering of stratospheric circulation by changing amounts of tropical ozone: A Pinatubo case study, *Geophys. Res. Lett.*, *19*, 1927-1930, 1992.

Kirchner, I., and H.-F. Graf, Volcanoes and El Niño: Signal separation in northern hemisphere winter, *Clim. Dyn.*, *11*, 341-358, 1995.

Kodera, K., Influence of volcanic eruptions on the troposphere through stratospheric dynamical processes in the northen hemisphere winter, *J. Geophys. Res.*, *99*, 1273-1282, 1994.

Kodera, K., M. Chiba, and K. Shibata, A general circulation model study of the solar and QBO modulation of the stratospheric circulation during the northern hemisphere winter, *Geophys. Res. Lett.*, *18*, 1209-1212, 1991.

Lacis, A. A., and M. I. Mishchenko, Climate forcing, climate sensitivity, and climate response: A radiative modeling perspective on atmospheric aerosols, in *Aerosol Forcing of Climate*, edited by R. J. Charlson and J. Heintzenberg, pp. 11-42, John Wiley, New York, 1995.

Mao, J., and A. Robock, Surface air temperature simulations by AMIP general circulation models: Volcanic and ENSO signals and systematic errors, *J. Clim.*, *11*, 1538-1552, 1998.

Minnis, P., E. F. Harrison, L. L. Stowe, G. G. Gibson, F. M. Denn, D. R. Doelling Jr., and W. L. Smith, Radiative climate forcing by the Mount Pinatubo eruption, *Science*, *259*, 1411-1415, 1993.

Morcrette, J.-J., Sur la parameterisation du rayonnement dans les modeles de la circulation generale atmospherique, Ph.D. thesis, Univ. of Lille, Lille, France, 1984.

Morcrette, J.-J., and Y. Fouquart, On systematic errors in parametrized calculations of longwave radiation transfer, *Q. J. R. Meteorol. Soc.*, *111*, 691-708, 1985.

Morcrette, J.-J., L. Smith, and Y. Fouquart, Pressure and temperature dependence of the absorption in longwave radiation parameterizations, *Contrib. Atmos. Phys.*, *59*, 455-469, 1986.

Naujokat, B., An update of the observed quasi-biennial oscillation of the stratospheric winds over the tropics, *J. Atmos. Sci.*, *43*, 1873-1877, 1986.

Pawson, S., K. Labitzke, R. Lenshow, B. Naujokat, B. Rajiwski, M. Wiesner, and R.-C. Wohlfart, Meteorologische Abhandlungen, Band 7, Heft 3, *Climatology of the Northern Hemisphere Stratosphere derived from Berlin Analyses, Part 1, Monthly Means*, 299 pp., Verlag von Dietrich Reimer, Berlin, 1993.

Perlwitz, J., and H.-F. Graf, The statistical connection between tropospheric and stratospheric circulation of the northern hemisphere in winter, *J. Clim.*, *8*, 2281-2295, 1995.

Reynolds, R. W., A real-time global sea surface temperature analysis, *J. Clim.*, *1*, 75-86, 1988.

Robock, A., and M. P. Free, Ice cores as an index of global volcanism from 1850 to the present, *J. Geophys. Res.*, *100*, 11,549-11,567, 1995.

Robock, A., and J. Mao, Winter warming from large volcanic eruptions, *Geophys. Res. Lett.*, *19*, 2405-2408, 1992.

Robock, A., and J. Mao, The volcanic signature in surface temperature observations, *J. Clim.*, *8*, 1086-1103, 1995.

Robock, A., K. E. Taylor, G. L. Stenchikov, and Y. Liu, GCM evaluation of a mechanism for El Niño triggering by the El Chichón ash cloud, *Geophys. Res. Lett.*, *22*, 2369-2372, 1995.

Roeckner, E., K. Arpe, L. Bengtsson, M. Christoph, M. Claussen, L. Dümenil, M. Esch, M. Giorgetta, U. Schlese, and U. Schullzweida, The atmospheric general circulation model ECHAM-4: Model description and simulation of present-day climate, MPI Rep. 218, 90 pp., Max Planck Inst. Meteorol., Hamburg, Germany, 1996a.

Roeckner, E., J.-M. Oberhuber, A. Bacher, M. Christoph, and I. Kirchner, ENSO variability and atmospheric response in a global coupled atmosphere-ocean GCM, *Clim. Dyn.*, *12*, 737-754, 1996b.

Rosenfield, J., D. Considine, P. Meade, J. Bacmeister, C. Jackman, and M. Schoeberl, Stratospheric effects of Mount Pinatubo aerosol studied with a coupled two-dimensional model, *J. Geophys. Res.*, *102*, 3649-3670, 1997.

Russell, P. B., et al., Pinatubo and pre-Pinatubo optical depth spectra: Mauna Loa measurements, comparisons, inferred particle size distributions, radiative effects, and relationship to lidar data, *J. Geophys. Res.*, *98*, 22,969-22,985, 1993.

Solomon, S., R. W. Portmann, R. R. Garcia, L. W. Thomason, L. R. Poole, and M. P. McCormick, The role of aerosol variations in anthropogenic ozone depletion at northern midlatitudes, *J. Geophys. Res.*, *101*, 6713-6727, 1996.

Stenchikov, G. L., I. Kirchner, A. Robock, H.-F. Graf, J. C. Antuña, R. G. Grainger, A. Lambert, and L. Thomason, Radiative forcing from the 1991 Mount Pinatubo volcanic eruption, *J. Geophys. Res.*, *103*, 13,837-13,857, 1998.

Stendel, M., and L. Bengtsson, Toward monitoring the tropospheric temperature by means of a general circulation model, *J. Geophys. Res.*, *102*, 29,779-29,788, 1997.

Tabazadeh, A., and R. P. Turco, Stratospheric chlorine injection by volcanic eruptions: HCl scavenging and implication for ozone, *Science*, *260*, 1082-1086, 1993.

Tie, X., and G. Brasseur, The response of stratospheric ozone to volcanic eruptions: Sensitivity to atmospheric chlorine loading, *Geophys. Res. Lett.*, *22*, 3035-3038, 1995.

Tie, X., G. P. Brasseur, C. Granier, A. De Rudder, and N. Larsen, Model study of polar stratospheric clouds and their effect on stratospheric ozone, 2, Model results, *J. Geophys. Res.*, *101*, 12,575-12,584, 1996.

Wentz, F. J., and M. Schabel, Effects of orbital decay on satellite-derived lower-tropospheric temperature trends, *Nature*, *394*, 661-664, 1998.

Wiscombe, W., Improved Mie scattering algorithms, *Appl. Opt.*, *190*, 1505-1509, 1980.

Zerefos, C. S., K. Tourpali, and A. F. Bais, Further studies on possible volcanic signal to the ozone layer, *J. Geophys. Res.*, *99*, 25,741-25,746, 1994.

J. C. Antuña, A. Robock, and G. L. Stenchikov (corresponding author), Department of Environmental Sciences, Rutgers - The State University of New Jersey, 14 College Farm Road, New Brunswick, NJ 08901-8551. (e-mail: antuna@envsci.rutgers.edu; robock@envsci.rutgers.edu; gera@envsci.rutgers.edu)

H.-F. Graf and I. Kirchner, Max-Planck-Institut für Meteorologie, Bundestrasse 55, D-20146 Hamburg, Germany. (e-mail: graf@dkrz.de; kirchner@dkrz.de)

(Received June 5, 1998; revised December 8, 1998; accepted March 29, 1999.)